Hindawi
International Journal of Aerospace Engineering
Volume 2022, Article ID 9913739, 13 pages
https://doi.org/10.1155/2022/9913739

Research Article

Study on the Cavitation Suppression Mechanism of Axial Piston Pump

Song Yan, Yi Jiang, and Mengya Hu

School of Aerospace Engineering, Beijing Institute of Technology, Beijing 100081, China

Correspondence should be addressed to Yi Jiang; 2449823572@qq.com

Received 6 September 2022; Revised 1 November 2022; Accepted 2 November 2022; Published 23 November 2022

Academic Editor: Chuang Liu

Gaseous and vaporous cavitation is extremely harmful to axial piston pumps, such as reducing flow rate, increasing flow pulsation, increasing vibration, increasing noise, and shortening life. To suppress the cavitation and improve the performance of axial piston pumps, a mathematical model for suppressing cavitation in the plunger chamber with a constant theoretical flow rate is innovatively established by combining the flow equation of the plunger pump and the pressure drop equation of the plunger chamber. Based on the model, two methods to suppress cavitation in the plunger chamber under the condition of a constant theoretical flow rate are proposed. The first method is to increase the distribution circle radius and correspondingly reduce the rotation speed, and the second method is to increase the plunger chamber radius and correspondingly reduce the rotation speed. To verify the effectiveness of these two methods, the CFD model of the axial piston pump is established, and the correctness of the model is verified by experiments. The results show that the two methods can effectively suppress cavitation in the plunger chamber, improve the actual flow rate, and reduce the flow pulsation under the condition of a constant theoretical flow rate. The research results can provide an important reference for the design and optimization of the plunger pump.

1. Introduction

Axial piston pumps are one of the positive displacement hydraulic pumps, which can convert mechanical power into hydraulic power. They are widely used in aerospace, machinery, ships, and other fields because of their compact structure, high functional density, high reliability, easy automation, and long life [1, 2].

Cavitation is a dynamic process where vapor bubbles form in the liquid when the localized pressure drops below the vapor pressure and then collapse when the localized pressure rises above the vapor pressure [3, 4]. In recent years, cavitation has been observed in plunger pumps, and the plunger chamber and the relief groove are the main areas where cavitation occurs [5–10]. When the bubbles generated by vaporous cavitation collapse, severe pressure fluctuation, pressure impact, and high-speed jet flow will be generated [11–13], accompanied by vibration and noise [14–18], which will lead to the formation of pits on the metal surface [19, 20]. The hydraulic oil is contaminated by the chipped metal particles, which further causes particle wear, resulting in a decrease in the sealing and load-bearing capacity of the friction pair. The air bubbles generated by the gaseous cavitation destroy the continuity of the oil discharge of the plunger pump, which leads to the reduction of the effective delivery flow rate and the decrease of the volumetric efficiency of plunger pumps [21–23].

Suppressing cavitation in the plunger chamber has always been one of the goals of scholars at home and abroad. Research shows that pressure drop is the main cause of cavitation in the plunger chamber [12, 24]. Two factors cause pressure drop are as follows: the first is the pressure loss along the way during the oil suction process of the plunger chamber [25, 26]. The second is the pressure drop near the center of rotation caused by centrifugal force when the plunger chamber rotates around the shaft [27, 28].

The plunger chamber is the most important hydraulic oil transmission area of the plunger pump. Therefore, the cavitation in the plunger chamber should be suppressed. At present, the main methods for suppressing cavitation in

the plunger chamber are as follows: the first method is to increase oil suction pressure. In this method, the initial pressure energy of hydraulic oil is increased by adding a turbine-increasing device at the oil suction port, which prevents the oil pressure from being affected by the energy loss along the way during the oil suction process, and finally achieves the purpose of suppressing cavitation [28, 29]. The second method is to decrease the oil discharge pressure [30]. This method can suppress cavitation by reducing the jet flow and backflow during the high-pressure and low-pressure conversion of the plunger chamber. The third method is to optimize the suction pipeline. This method can effectively reduce the suction pressure drop and achieve the purpose of suppressing cavitation by keeping the oil suction direction of the oil suction pipeline consistent with the tangential velocity direction of the plunger chamber [31–33]. The fourth method is to reduce the rotation speed. The method can suppress cavitation in the plunger chamber by reducing pressure difference and increasing the pressure near the inside wall of the plunger chamber [12, 34]. The fifth method is to reduce the swash plate inclination angle. The method can reduce the oil suction force by reducing the relative axial speed, thereby reducing the energy loss along the way and suppressing cavitation in the plunger chamber [35].

Although some achievements have been made in suppressing cavitation in the plunger chamber, there are still some shortcomings. For example, the theoretical flow rate will decrease when decreasing the rotation speed or decreasing the swash plate inclination angle.

Faced with the problem that reducing the rotation speed or decreasing the swash plate inclination angle will reduce the theoretical flow rate, in this paper, the pressure drop equation of the plunger chamber is deduced, and by combining the theoretical flow equation of the plunger pump and the pressure drop equation of the plunger chamber, the pressure drop model of the plunger chamber with an invariable theoretical flow rate is innovatively established. Based on this model, the measures to suppress cavitation in the plunger chamber with a constant theoretical flow rate are proposed and verified. The results can provide an important reference for suppressing cavitation in the plunger chamber.

2. Model Derivation of Pressure Drop in Plunger Chamber under Constant Theoretical Flow Rate

During the operation of the plunger pump, the viscosity and compressibility can be ignored because the hydraulic oil flow rate is extremely fast and the oil will not be subject to the high pressure during the normal oil suction process. Consider a fluid particle P that flows from the suction port to the plunger chamber. For inviscid flow, Euler's equations can be expressed in vector notation as

$$\rho \frac{\mathrm{D}\vec{\mathrm{v}}}{\mathrm{Dt}} = \rho\vec{g} - \nabla p, \tag{1}$$

where $\rho$is the fluid density, $\vec{\mathrm{v}}$ is the velocity of the fluid particle, $\vec{\mathrm{g}}$ is the body force, and p is the pressure at an arbitrary location in the cylinder chamber.

Because the plunger chamber pressure drop model needs to be studied from an analytical equation point of view, the hydraulic oil flow is assumed to be steady state.

$$\frac{\mathrm{Dv}}{\mathrm{Dt}} = \frac{\partial \vec{v}}{\partial t} + \left(\vec{v}\bullet\nabla\right)\vec{v} = \left(\vec{v}\bullet\nabla\right)\vec{v} = \nabla\left(\frac{1}{2}v^2\right) + \left(\nabla\times\vec{v}\right)\times\vec{v}. \tag{2}$$

By combining Equations (1) and (2), Equation (1) can be rewritten as

$$\nabla\left(\frac{1}{2}v^2\right) + \left(\nabla\times\vec{v}\right)\times\vec{v} = \vec{g} - \frac{1}{\rho}\nabla p. \tag{3}$$

Because the axial piston pump is a rotating fluid machine, the Cartesian coordinate system should be converted into a cylindrical coordinate system. The origin and z-axis of the cylindrical coordinate system coincide with the origin and z-axis of the Cartesian coordinate system, respectively. Figure 1 shows the schematic diagram of the oil location in the plunger chamber. The blue coordinate is the local coordinate system, the distance between the fluid particle P in the plunger chamber and the origin of the cylindrical coordinate system is R_s, and the distance between the fluid particle P and the origin of the local coordinate system is r_p. According to the geometric structure of the plunger pump and the rotating cylindrical coordinate system, R_s can be expressed as

$$R_s = \sqrt{R^2 + r_p^2 + 2r_pR\cos\left(\theta_p\right)}, \tag{4}$$

where θ_{p} is s measured from the Ys-axis and the clockwise rotation is supposed to be positive.

Compared with the centrifugal force on the fluid particle, the gravity is very small and can be ignored. In the rotating cylindrical coordinate system, Equation (3) can be written as

$$\nabla\left(\frac{1}{2}v_R^2\right) + \left(\nabla\times v_R\right)\times v_R = -w\times\left(w\times R_s\right) - \dot{w}\times R_s - 2w\times v_R - \frac{1}{\rho}\nabla p. \tag{5}$$

Considering that the cylinder is constantly rotating and w is parallel to v_R, Equation (5) can be expressed as

$$\nabla\left(\frac{1}{2}v_R^2\right) + \left(\nabla\times v_R\right)\times v_R = -w\times\left(w\times R_s\right) - \frac{1}{\rho}\nabla p. \tag{6}$$

Through transformation, Equation (6) can be written as

$$\nabla\left(\frac{1}{2}v_R^2\right) + \left(\nabla\times v_R\right)\times v_R = \nabla\left(\frac{w^2R_s^2}{2}\right) - \frac{1}{\rho}\nabla p. \tag{7}$$

Taking the dot product of each term with ds along the

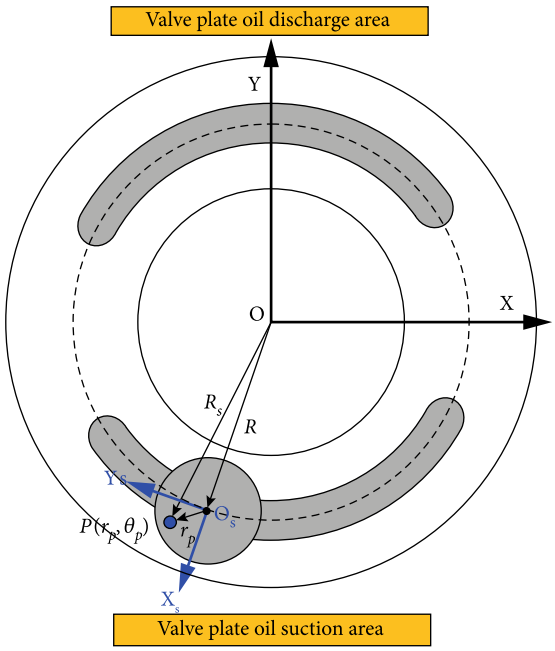

Figure 1: Schematic diagram of oil location in plunger chamber.

streamline, Equation (7) can be written as

$$\nabla\left(\frac{1}{2}v_R^2\right)\bullet \mathrm{ds} + (\nabla \times v_R) \times v_R \bullet \mathrm{ds} = \nabla\left(\frac{w^2 R_s^2}{2}\right)\bullet ds - \frac{1}{\rho}\nabla p \bullet \mathrm{ds}. \tag{8}$$

Considering $\nabla(1/2v_R^2) \cdot \mathrm{ds} = 0$ and $(\nabla \times v_R) \times v_R \cdot \mathrm{ds} = 0$, Equation (8) can be expressed as

$$d\left(\frac{1}{2}v_R^2\right) = d\left(\frac{w^2 R_s^2}{2}\right) - \frac{1}{\rho}\nabla p. \tag{9}$$

Equation (9) can be integrated along the streamline direction to obtain the streamline equation

$$\frac{1}{2}\rho v_R^2 = \frac{\rho w^2 R_s^2}{2} - p + c, \tag{10}$$

where c is the integral constant. Considering two situations of hydraulic oil, the first is when the fluid particle flows from the valve plate into the cylinder block, and the second is when the fluid particle reciprocates in the plunger chamber, and the following two expressions can be obtained according to Equation (10).

$$\frac{1}{2}\rho v_{\mathrm{in}}^2 = \frac{\rho w^2 R^2}{2} - p_{\mathrm{in}} + c_1, \tag{11}$$

$$\frac{1}{2}\rho v_p^2 = \frac{\rho w^2 R_s^2}{2} - p_p + c_2, \tag{12}$$

where v_{in} and p_{in} are the velocity and pressure of the fluid particle at the oil suction port of the valve plate, respectively, v_p and p_p are the flow rate and pressure of the fluid particle in the plunger chamber, respectively, r_p is the distance between the fluid particle in the plunger chamber and the center of the plunger chamber window.

During the oil suction stage of the plunger chamber, the velocity of the fluid particle relative to the rotating cylinder block can be expressed as

$$v_p \approx v_i = \mathrm{wRtan}\beta \sin(\mathrm{wt}), \tag{13}$$

where v_i is the axial velocity of the plunger. The inlet pressure p_l can be obtained if the flow resistance from the pump inlet to the valve-plate suction port is neglected.

$$p_l = p_{\mathrm{in}} + \frac{1}{2}\rho v_{\mathrm{in}}^2, \tag{14}$$

where p_l is the inlet pressure of the plunger pump.

The cylinder pressure at an arbitrary location can be obtained by combining Equations (11)–(14).

$$p_p = p_{\mathrm{in}} + \frac{1}{2}\rho v_{\mathrm{in}}^2 + \frac{1}{2}\rho w^2\left(R_s^2 - R^2\right) - \frac{1}{2}\rho c_1[\mathrm{wRtan}\beta \sin(wt)]^2, \tag{15}$$

where c_1 is the damping coefficient of the cylinder block window. The damping flow equation is expressed as

$$q_d = A_{\mathrm{cw}} C_v \sqrt{\frac{2\left(p_{\mathrm{plate}} - p_p\right)}{\rho}}, \tag{16}$$

$$q_d = v_p \pi r^2, \tag{17}$$

where P_{plate} is the pressure of fluid particle in the valve plate, q_d is the flow rate under the damping action, A_{cw} is the cylinder block window area. Equation (18) can be obtained by combining Equations (16) and (17).

$$p_{\mathrm{plate}} - p_p = v_p^2 \frac{\rho\left(\pi r^2\right)^2}{2A_{\mathrm{cw}}^2 C_v^2}. \tag{18}$$

The formula of the pressure drop-damping coefficient c_1 of the cylinder block window can be expressed as

$$c_1 = \frac{\left(\pi r^2\right)^2}{A_{\mathrm{cw}}^2 C_v^2}. \tag{19}$$

Then, Equation (15) can be written as

$$p_p = p_{\mathrm{in}} + \frac{1}{2}\rho v_{\mathrm{in}}^2 + \frac{1}{2}\rho w^2\left(R_s^2 - R^2\right) - \frac{1}{2}\rho w^2 \frac{\left(\pi r^2\right)^2}{A_{\mathrm{cw}}^2 C_v^2}[R \tan\beta \sin(wt)]^2. \tag{20}$$

The relationship between the pressure at an arbitrary location in the plunger chamber and the pressure at the

suction port of the plunger pump can be expressed as

$$p_p = p_l - \frac{1}{2}\rho w^2\left[c_1 R^2 \tan^2\beta \sin^2(wt) - \left(r_p^2 + 2r_p R\cos\theta_p\right)\right]. \tag{21}$$

According to Equation (21), the pressure p_1 of the oil suction port and the overall pressure drop coefficient c_2^1 are the factors that affect the pressure in the plunger chamber. The overall pressure drop coefficient includes c_3 and c_4, c_3 is the pressure drop coefficient caused by the loss along the way during the oil suction process of the plunger chamber, and c_4 is the centrifugal pressure drop coefficient caused by the centrifugal force.

$$c_2^1 = c_1 R^2 \tan^2\beta \sin^2(wt) - \left(r_p^2 + 2r_p R\cos\theta_p\right), \tag{22}$$

$$c_3 = c_1 R^2 \tan^2\beta \sin^2(wt), \tag{23}$$

$$c_4 = -\left(r_p^2 + 2r_p R\cos\theta_p\right). \tag{24}$$

In the equations, sin (wt) = 0 means that the plunger chamber is at the dead center position of the distribution circle, sin (wt) = 1 means that the plunger chamber is in the middle of the two dead centers of the distribution circle, cos $(\theta_p) = -1$ means that the fluid particle is at the near rotation center of the plunger chamber, cos $(\theta_p) = 1$ means that the fluid particle is at the far rotation center of the plunger chamber. The pressure drop usually occurs at the near rotation center of the plunger chamber, while the pressure increase occurs at the far rotation center, so only the case of the near rotation center ($r_p = r$ and cos $(\theta_p) = -1$) is considered. The pressure drop coefficient c_3 of the loss along the way is the largest when the plunger chamber is located in the middle of the upper and lower dead centers, so only the case of sin (wt) = 1 needs to be considered. To sum up, the centrifugal pressure drop coefficient c_4 can be expressed as

$$c_4 = 2\mathrm{rR} - r^2. \tag{25}$$

The overall pressure drop coefficient c_2^1 can be rewritten as

$$c_2 = c_1 R^2 \tan^2\beta + 2\mathrm{rR} - r^2. \tag{26}$$

Taking the fluid particle at the near rotation center of the 90° plunger chamber as the research object, the pressure drop formula can be expressed as

$$p_p = p_l - \frac{1}{2}\rho w^2\left(c_1 R^2 \tan^2\beta + 2\mathrm{rR} - r^2\right). \tag{27}$$

In order to suppress cavitation in the plunger chamber, it is necessary to increase the pressure in the plunger chamber by reducing the pressure drop coefficient C.

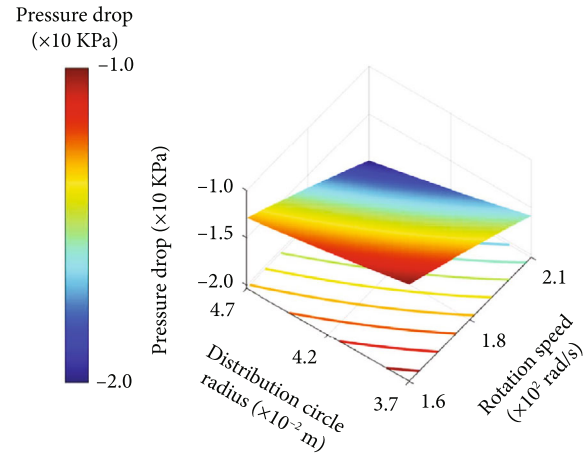

Figure 2: The relationship between the distribution circle radius R, the rotation speed w, and the variable pressure drop term c_6.

$$C = \frac{1}{2}\rho w^2\left(c_1 R^2 \tan^2\beta + 2\mathrm{rR} - r^2\right). \tag{28}$$

According to Equation (28), the pressure drop can be suppressed by four methods, which are reducing the swash plate inclination angle β, reducing the cylinder rotation speed w, reducing the distribution circle radius R, and reducing the plunger chamber radius r.

Although the cavitation in the plunger chamber can be effectively suppressed by reducing the rotation speed, reducing the swash plate inclination angle, reducing the distribution circle radius, and reducing the plunger chamber radius, the theoretical flow rate, the most key parameter of a plunger pump, will decrease by these methods to suppress cavitation. To solve this problem, it is necessary to suppress cavitation in the plunger chamber based on the constant theoretical flow rate. Because the flow rate of the axial piston pump is determined by the flow rate of a single plunger chamber, the theoretical flow rate formula of a single plunger chamber is introduced here.

$$Q_i = \pi r^2 \mathrm{wRtan}\beta \sin(wt). \tag{29}$$

Because the theoretical flow rate of the axial piston pump is not affected by sin (wt), sin (wt) = 1 is considered. Through simplification, the theoretical flow formula of a single plunger chamber can be expressed as

$$Q_i = \pi r^2 \mathrm{wRtan}\beta. \tag{30}$$

According to Equation (30), the four variable parameters are the plunger chamber radius r, the cylinder rotation speed w, the distribution circle radius R, and the swash plate inclination angle β. In order to keep the theoretical flow constant, the following two cases can be considered, namely, R × w = const1 and r^2 × w = const2.

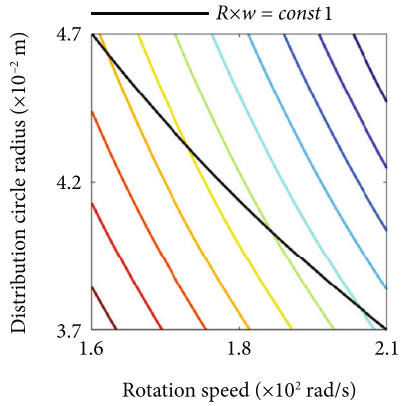

Figure 3: The projected contour plot of the variable pressure drop term c_6 on the R-w plane.

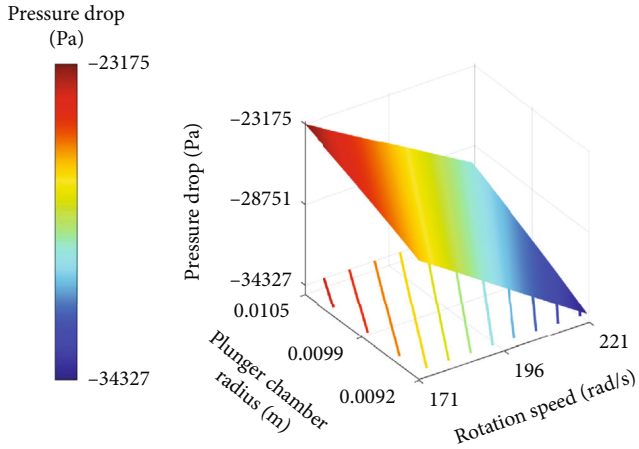

Figure 4: The relationship curves between the plunger chamber radius, the rotation speed, and the variable pressure drop term.

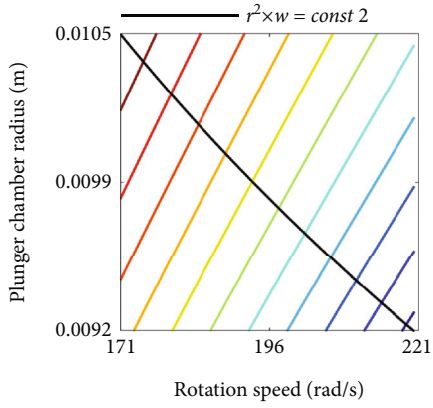

Figure 5: The projected contour plot of the variable pressure drop term c_6 on the r × w plane.

By transforming Equation (30), it can be rewritten as

$$R = \frac{Q_i}{\pi r^2 w \tan\beta}. \tag{31}$$

Substituting Equation (31) into Equation (26), Equation (26) can be rewritten as

$$c_2 = \frac{\rho(\pi r^2)^2}{2A_{cw}^2 C_v^2}\left(\frac{Q_i}{\pi r^2 w \tan\beta}\right)^2 \tan^2\beta + \left(2r\frac{Q_i}{\pi r^2 w \tan\beta} - r^2\right). \tag{32}$$

By simplification, Equation (32) can be rewritten as

$$c_2 = \frac{\rho}{2A_{cw}^2 C_v^2}\left(\frac{Q_i}{w}\right)^2 + 2\frac{Q_i}{\pi r w \tan\beta} - r^2. \tag{33}$$

By combining Equations (27) and (33), the pressure drop equation of the 90° plunger chamber at the near rotation center can be expressed as

$$p_p = p_l - \frac{\rho Q_i^2}{2A_{cw}^2 C_v^2} - \frac{\rho w Q_i}{\pi r \tan\beta} + \frac{1}{2}\rho w^2 r^2. \tag{34}$$

According to Equation (34), the fixed pressure drop term c_5 and the variable pressure drop term c_6 are the two-plunger chamber pressure drop terms related to the plunger chamber radius and the distribution circle radius. The expressions for c_5 and c_6 are Equations (35) and (36), respectively

$$c_5 = -\frac{\rho Q_i^2}{2A_{cw}^2 C_v^2}, \tag{35}$$

$$c_6 = \frac{1}{2}\rho w^2 r^2 - \frac{\rho w Q_i}{\pi r \tan\beta}. \tag{36}$$

Because the influence of the distribution circle radius R on the variable pressure drop term c_6 needs to be studied, by combining Equations (30) and (36), Equation (36) can be rewritten as

$$c_6 = \frac{1}{2}\frac{\rho w Q_i}{\pi R \tan\beta} - \rho w\sqrt{\frac{wRQ_i}{\pi \tan\beta}}. \tag{37}$$

Figure 2 shows the relationship curves between the distribution circle radius R, the rotation speed w, and the variable pressure drop term c_6. Figure 3 shows the projected contour plot of the variable pressure drop term c_6 on the R -w plane, and the black solid line is the relationship curve between the distribution circle radius R and the rotation speed w under the condition of constant oil discharge flow rate in this paper. Under the premise of R × w = const1, the variable pressure drop term $^{c}{}_{6}$ decreases as the distribution circle radius R increases. Therefore, under the condition of the constant theoretical flow rate, the cavitation in the plunger chamber can be suppressed by increasing the

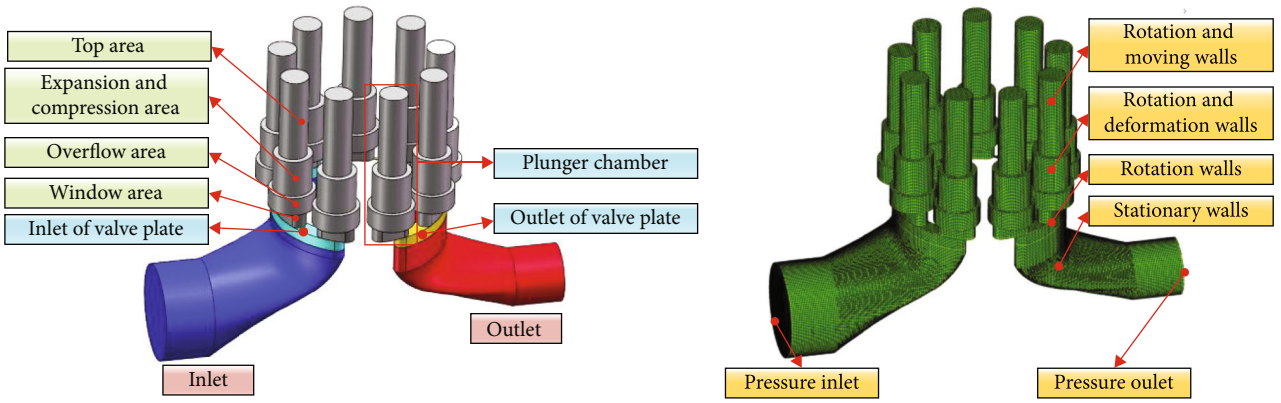

(a) Fluid domain model (b) Mesh model

Figure 6: Fluid domain model and mesh model of axial piston pump model.

Table 1: Geometric parameters of fluid domain model.

Parameters	Value	Parameters	Value
Number of plungers	9	The height of the top region (m)	0.0450
Plunger chamber radius (m)	0.01	Radius of the top region (m)	0.0075
The thickness of window region (m)	0.0094	The outer diameter of valve plate fluid field (m)	0.0445
The radius of the overflow region (m)	0.012	The inner diameter of the valve plate fluid domain (m)	0.0365
The radius of expansion and compression region (m)	0.01	Type of relief groove	Triangle

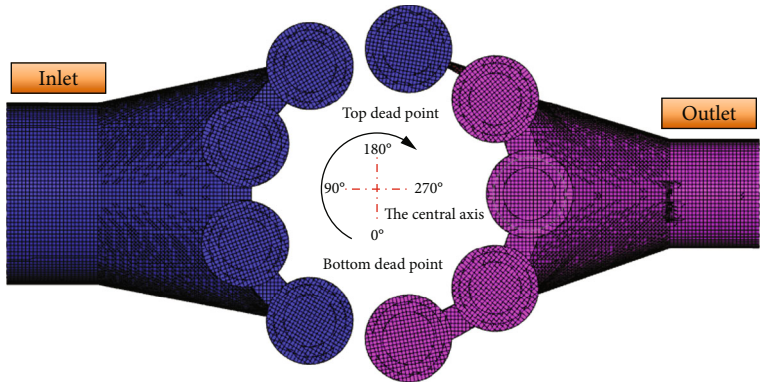

Figure 7: The fluid domain and mesh motion diagram of the plunger chamber.

Table 2: Input parameters of CFD simulation model.

Parameters	Value	Parameters	Value
Inlet pressure (Pa)	101325	Residual convergence	1×10^{-3}
Outlet pressure (Mpa)	20	Fluid density (kg/m^3)	837
Viscosity (Pa·s)	1.003×10^{-3}	Bulk modulus of elasticity (MPa)	1.5×10^3
Gas mass fraction	9×10^{-5}	Tangent of swashplate inclination	0.23617395
Rotation speed (r/min)	1800	Revolutions	15
Saturated vapor pressure (MPa)	4×10^{-4}	Iterations per step	150

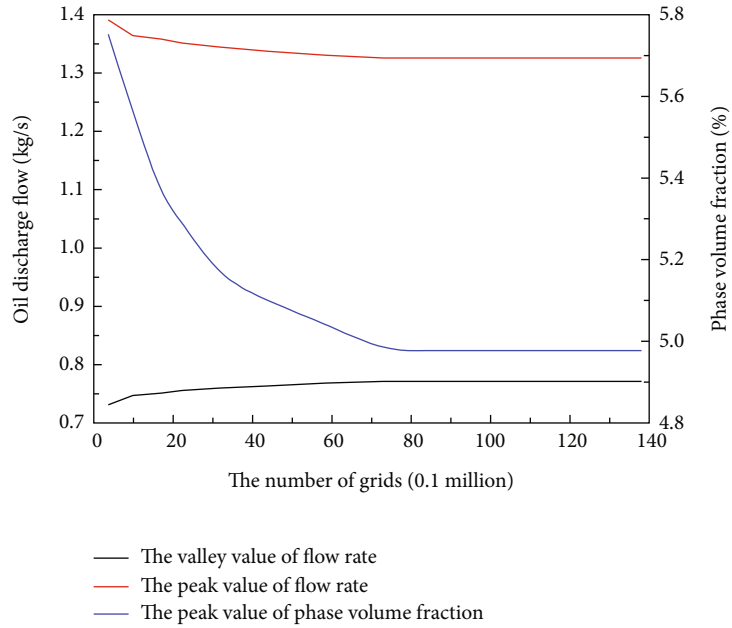

Figure 8: The variation curves of three characteristic parameters with the number of grids.

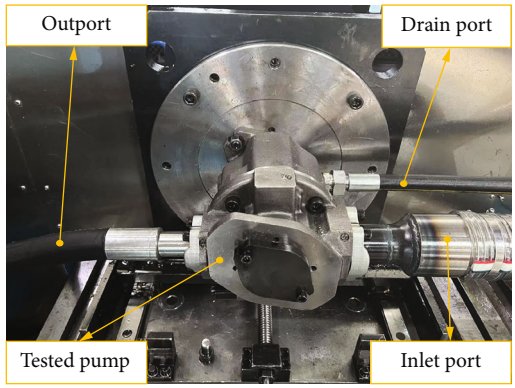

Figure 9: The tested axial plunger pump.

distribution circle radius and correspondingly reducing the rotation speed.

Considering $r^2 \times w = const2$, Equation (38) can be written as

$$c_6 = \frac{1}{2}\rho w \times const2 - \frac{\rho w Q_i}{\pi r \tan \beta}. \quad (38)$$

Figure 4 shows the relationship curves between the plunger chamber radius r, the rotation speed w, and the variable pressure drop term c_6. Figure 5 shows the projected contour plot of the variable pressure drop term c_6 on the $r \times w$ plane, and the black solid line is the relationship curve between the plunger chamber radius r and the rotation speed w under the condition of a constant oil discharge flow rate. Under the premise of $r^2 \times w = const2$, the variable pressure drop term c6 decreases as the plunger chamber radius r increases. Therefore, under the condition of a constant theoretical flow rate, the cavitation in the plunger chamber

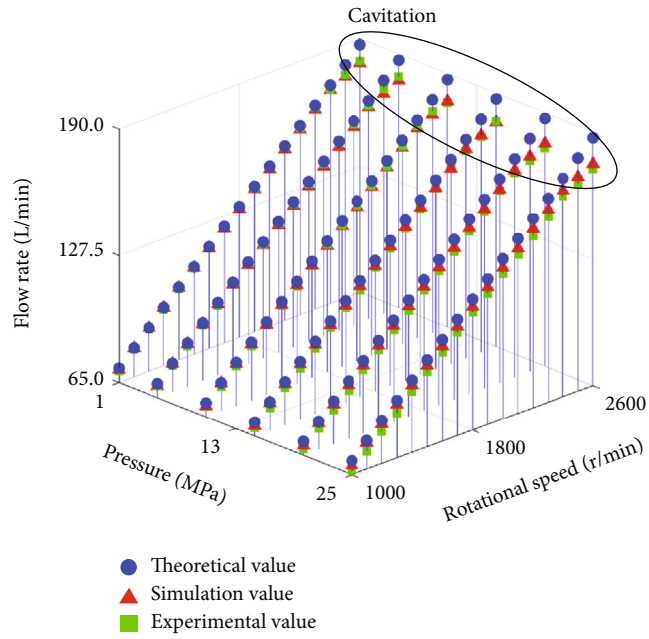

Figure 10: Comparison of theoretical flow rate, simulated flow rate, and experimental flow rate under different pressure and rotation speed conditions.

can be suppressed by increasing the plunger chamber radius and correspondingly reducing the rotation speed.

Flow pulsation is one of the key indicators to evaluate the performance of the axial plunger pump. Assuming δ is the flow pulsation, then δ can be expressed as

$$\delta = \frac{Q_{max} - Q_{min}}{1/2(Q_{max} + Q_{min})}, \quad (39)$$

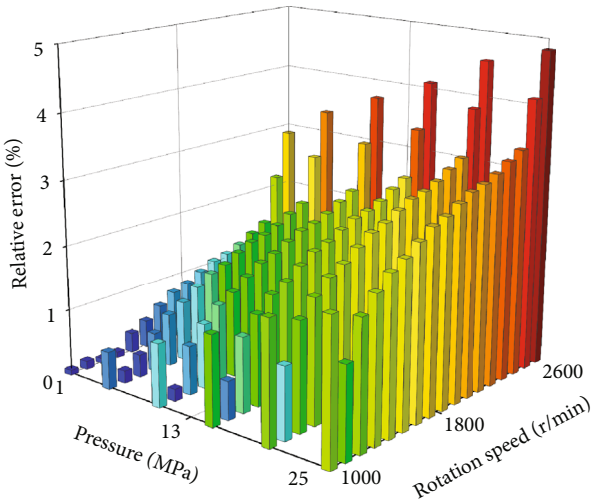

Figure 11: The relative error between theoretical results and simulation results.

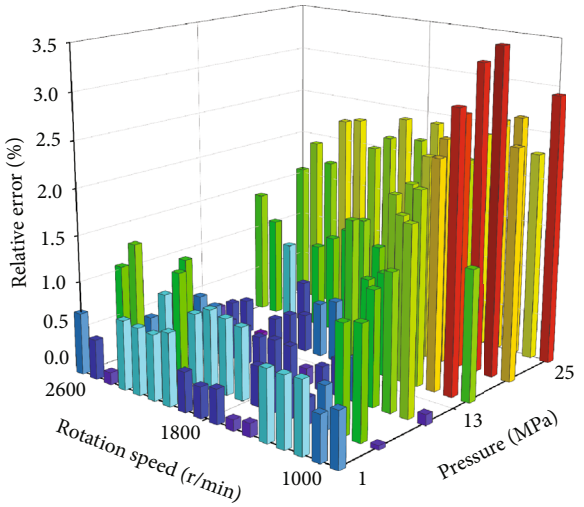

Figure 12: The relative error between simulation results and experiment results.

where Q_{max} is the maximum instantaneous flow rate and Q_{min} is the minimum instantaneous flow rate.

3. Cavitation Suppression Simulation and Result Analysis in Plunger Chamber

3.1. CFD Model. Figure 6 shows the fluid domain model and mesh model of the plunger pump. Because there is relative motion among the components of the axial piston pump during operation, the fluid domain of the piston pump is divided into 5 parts: inlet, outlet, inlet of valve plate, outlet of valve plate, and plunger chamber. To accurately locate the position of the plunger chamber, the plunger chamber is divided into four areas according to the order in which the hydraulic oil is sucked, which are the chamber window area, the chamber overflow area, the chamber expansion and compression area and the chamber top area. Table 1 shows the parameters of the fluid domain of the plunger

Table 3: Combination list of distribution circle radius and rotation speed.

Serial number	Distribution circle radius R (m)	Rotation speed w (r/min)	Const1 (mr/min)
1	0.036735	1984.500	72.9
2	0.038548	1891.125	72.9
3	0.040500	1800.00	72.9
4	0.042604	1711.125	72.9
5	0.044875	1624.500	72.9
6	0.047333	1540.125	72.9

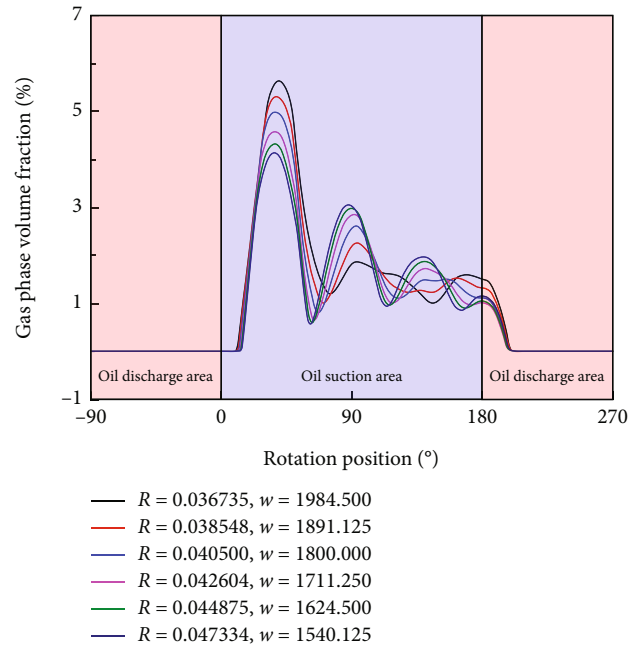

Figure 13: The gas phase volume fraction curves in the plunger chamber with different distribution circle radii and rotation speeds.

pump. The type of the relief groove is a triangular relief groove, and the type of the pump is a 9-piston variable displacement axial piston pump.

Figure 7 shows the fluid domain and mesh motion diagram of the plunger chamber. The fluid domain of the axial piston pump is divided by the Cartesian grid, which has the advantages of high accuracy, fast speed, less grid quantity demand, and high flow field resolution. The meshed parts are connected by a Mismatched Grid Interface (MGI), which is treated as the common face connecting cells on both sides of the interface. During the simulation process, the interface is the same as an internal interface between two neighboring cells in the same grid domain.

In Figure 7, the bottom dead point is set to 0°, and the top dead point is set to 180°. In actual working conditions, the oil is sucked in when the plunger chamber rotates from 0° to 180°, the oil is discharged when the plunger chamber rotates from 180° to 360°. During the oil suction stage, the length of the plunger chamber increases regularly because the expansion and compression region of the plunger chamber is stretched. During the oil discharge stage, the length of

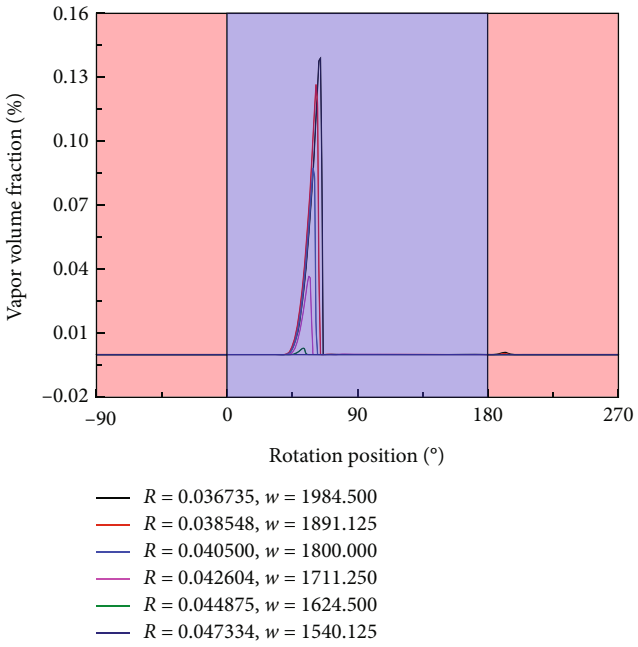

Figure 14: The vapor volume fraction curves in the plunger chamber with different distribution circle radii and rotation speeds.

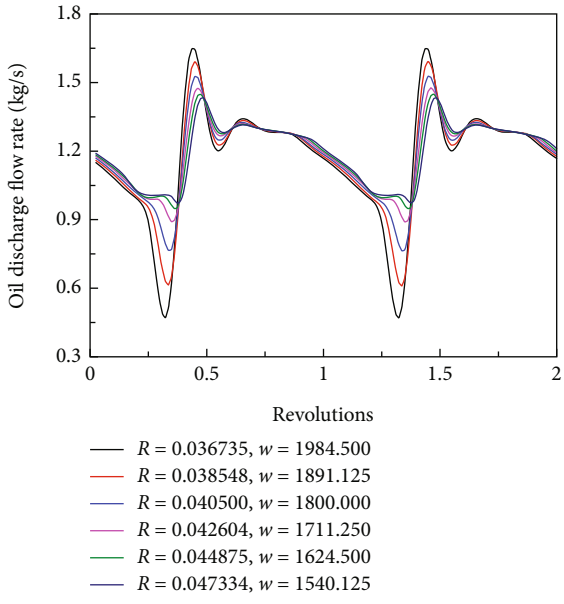

Figure 15: The flow rate curves of the outlet port with different distribution circle radii and rotation speeds.

the plunger chamber decreases regularly because the expansion and compression region is compressed.

The boundary conditions and fluid properties for the CFD model are shown as in Figure 6 and Table 2. During the operation of the plunger pump, the pressure, flow rate, and cavitation of the fluid will change with time. Therefore, the simulation type is unsteady, and the plunger chamber rotates by 1° in each iteration step. Before the simulation is started, the internal flow field of the plunger pump is in a static state, and after the simulation is started, the flow field

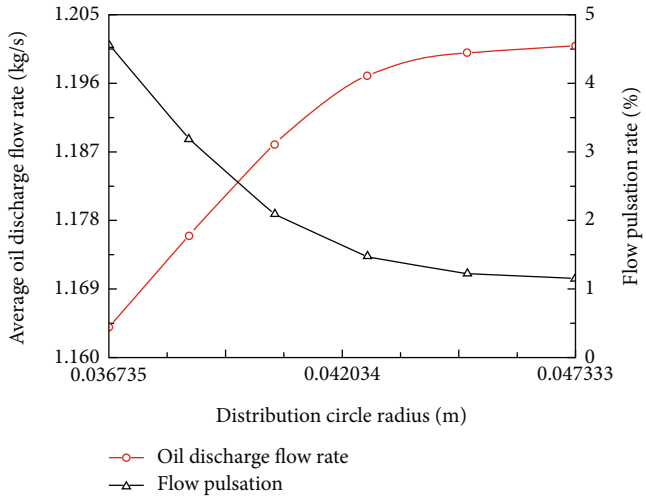

Figure 16: The average oil discharge flow rate curve and flow pulsation curve with different distribution circle radii and rotation speeds.

is in a turbulent state. After the plunger chamber rotates 13 times, the simulation results gradually become stable. Therefore, the total iteration step in this paper is 5400 steps, that is, the plunger chamber rotates 15 times in total. All the simulation results in this paper are the results after the flow field becomes stable. In the simulation model, the full cavitation model is selected as the cavitation model, and the standard k-ε turbulence model is selected as the turbulence model.

To verify that the simulation results are independent of the grid size, a working condition is selected for simulation, in which the pressure at the oil suction port is one atmosphere, the pressure at the oil discharge port is 20 Mpa, and the rotation speed is 1800 r/min.

In the study of suppressing cavitation in the plunger chamber, the characteristic parameters include the peak value of the gas phase volume fraction of the plunger chamber, the valley value of the flow rate, and the peak value of the flow rate. Figure 8 shows the variation curves of three characteristic parameters with the number of grids. When the number of grids is more than 500000, three characteristic parameters become stable. Therefore, to ensure the accuracy of the simulation results, the number of grids is 800000.

To verify the correctness of the simulation model, the flow rate of the plunger pump under the conditions of different pressures and rotation speeds is tested, and the tested axial plunger pump is shown in Figure 9.

Figure 10 shows the comparison of the theoretical flow rate, simulation flow rate and experimental flow rate of the plunger pump when P_{in} is equal to 0.5 Mpa. Figure 11 shows the relative error between theoretical results and simulation results; Figure 12 shows the relative error between simulation results and experiment results. From the point of view of pressure and rotation speed, the simulation flow rate is basically consistent with the experimental flow rate, the relative error between theoretical results and simulation results does not exceed 5% and the relative error between the simulation results and the experimental results does not exceed 3.5%, which verifies the correctness of the simulation model

Table 4: Combination list of plunger chamber radius and rotation speed.

Serial number	Plunger chamber radius r (m)	Rotation speed w (r/min)	const2 (m^2r/min)
1	0.01050	1632.653	0.18
2	0.01025	1713.265	0.18
3	0.01000	1800.000	0.18
4	0.00975	1893.491	0.18
5	0.00950	1994.459	0.18
6	0.00925	2103.725	0.18

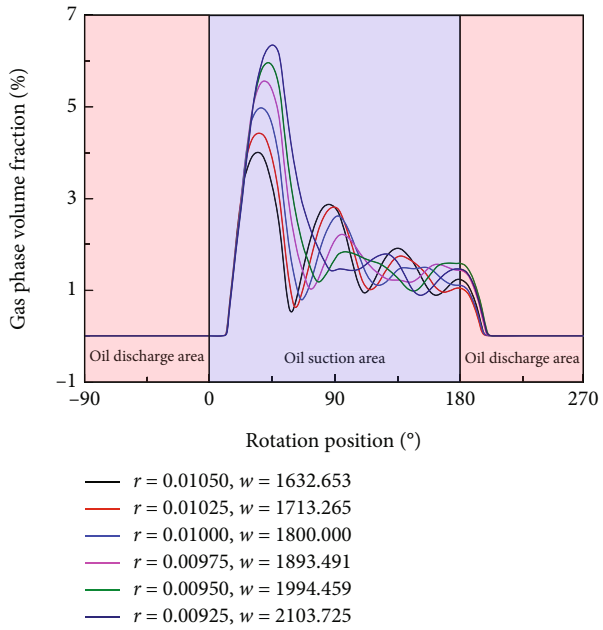

Figure 17: The curves of the gas phase volume fraction in the plunger chamber with different plunger chamber radii and rotation speeds.

of the plunger pump. The difference between the theoretical flow rate and the simulation flow rate increases with the increase of pressure, which is caused by the aggravation of backflow. The difference between the theoretical flow rate and the experimental flow rate increases with the increase of pressure, which is caused by the aggravation of backflow and leakage. The difference between the theoretical flow rate, the simulation flow rate, and the experimental flow rate increases with the increase of the rotation speed, which is caused by the increased cavitation caused by the increase of the rotation speed.

3.2. Cavitation Suppression Based on Distribution Circle Radius and Rotation Speed. In order to study the cavitation suppression in the plunger chamber based on distribution circle radius and rotation speed, 6 groups of data of distribution circle radius and rotation speed are selected, and the data are shown in Table 3.

Figure 13 shows the curves of the gas phase volume fraction in the plunger chamber with different distribution circle radii and rotation speeds. Under the condition of a constant

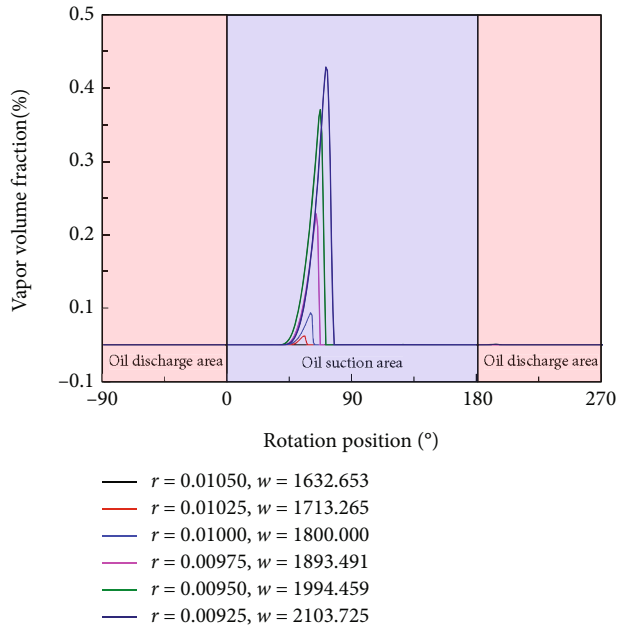

Figure 18: The curves of the vapor volume fraction in the plunger chamber with different plunger chamber radii and rotation speeds.

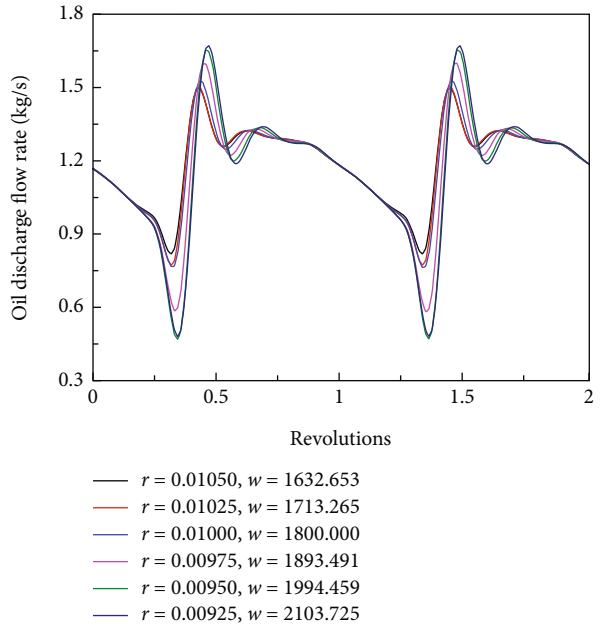

Figure 19: The flow rate curves of the outlet port with different plunger chamber radii and rotation speeds.

theoretical flow rate, the gas phase volume fraction in the plunger chamber decreases with the increase of the distribution circle radius. When the distribution circle radius increases from 0.036735 m to 0.047334 m, the peak value of the gas phase volume fraction in the plunger chamber decreases from 5.638% to 4.138%, and the average gas phase volume fraction decreases from 1.080% to 0.963%. Figure 14 shows the curves of the vapor volume fraction in the plunger chamber with different distribution circle radii and rotation speeds. Under the condition of a constant theoretical flow

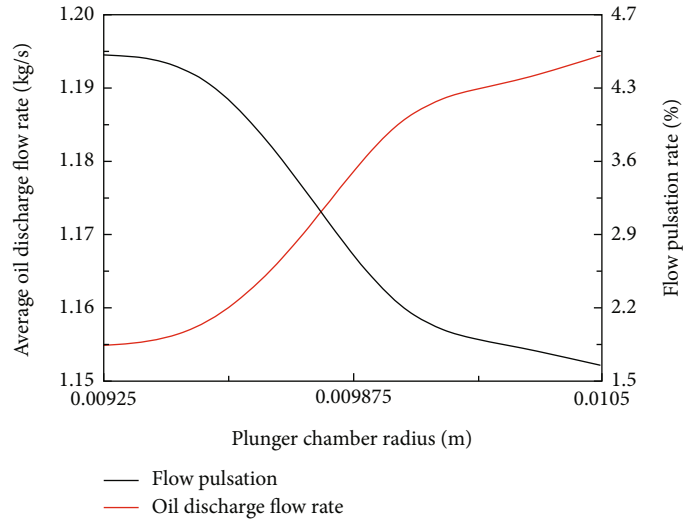

Figure 20: The average oil discharge flow rate carve and flow pulsation rate curve with different plunger chamber radii and rotation speeds.

rate, with the increase of the distribution circle radius and the corresponding decrease of the rotation speed, the vapor volume fraction in the plunger chamber decreases. When the distribution circle radius increases from 0.036735 m to 0.047334 m and the rotation speed decreases from 1984.5 r/min to 1540.125 r/min, the vapor volume fraction in the plunger chamber decreases from 0.139% to zero. To sum up, under the condition of a constant theoretical flow rate, the gaseous cavitation and vaporous cavitation in the plunger chamber can be effectively suppressed by increasing the distribution circle radius and correspondingly reducing the rotation speed.

Figure 15 shows the flow rate curves of the outlet port with different distribution circle radii and rotation speeds. With the increase of the distribution circle radius and the corresponding decrease of the rotation speed, the peak values of the outlet port flow rate decrease and the valley values increase, which plays the role of "cutting the peak and filling the valley." Under the condition of a constant theoretical flow rate, when the distribution circle radius increases from 0.036735 m to 0.047334 m, the peak value of the flow rate decreases from 1.642 kg/s to 1.432 kg/s, and the valley value increases from 0.474 kg/s to 0.972 kg/s. Figure 16 shows the average oil discharge flow rate curve and flow pulsation rate curve with different distribution circle radii and rotation speeds. By increasing the distribution circle radius, the cavitation in the plunger chamber can be suppressed, and the backflow and jet flow rate can be reduced, thereby increasing the actual flow rate and reducing the flow pulsation. When the distribution circle radius increases from 0.036735 m to 0.047333 m, the actual flow rate increases from 1.164 kg/s to 1.201 kg/s, and the flow pulsation rate decreased from 4.564% to 1.153%. To sum up, the actual flow rate can be effectively increased and the flow pulsation can be reduced by increasing the distribution circle radius and correspondingly reducing the rotation speed.

3.3. Cavitation Suppression Based on Plunger Chamber Radius and Rotation Speed. In order to study the cavitation suppression of the plunger chamber based on plunger chamber radius and rotation speed, 6 groups of data of plunger chamber radius and rotation speed are selected, and the data are shown in Table 4.

Figure 17 shows the curves of the gas phase volume fraction in the plunger chamber with different plunger chamber radii and rotation speeds. Under the condition of a constant theoretical flow rate, the gas phase volume fraction in the plunger chamber decreases with the increase of the plunger chamber radius. When the plunger chamber radius increases from 0.00925 m to 0.0105 m, the peak value of the gas phase volume fraction decreases from 6.348% to 4.010%, and the average gas phase volume fraction decreases from 1.186% to 0.942%. Figure 18 shows the curves of the vapor volume fraction in the plunger chamber with different plunger chamber radii and rotation speeds. Under the condition of a constant theoretical flow rate, with the increase of the plunger chamber radius and the corresponding decrease of the rotation speed, the vapor volume fraction in the plunger chamber decreases. When the plunger chamber radius increases from 9.25 mm to 10.5 mm, the vapor volume fraction decreases from 3.74% to zero. To sum up, under the condition of a constant theoretical flow rate, the gaseous cavitation and vaporous cavitation in the plunger chamber can be effectively suppressed by increasing the plunger chamber radius and correspondingly reducing the rotation speed.

Figure 19 shows the flow rate curves of the outlet port with different plunger chamber radii and rotation speeds. With the increase of the plunger chamber radius and the corresponding decrease of the rotation speed, the peak values of the outlet port flow rate decrease and the valley values increase, which plays the role of "cutting the peak and filling the valley." When the plunger chamber radius increases from 0.00925 m to 0.0105 m, the peak value of the oil discharge flow rate decreases from 1.66 kg/s to 1.49 kg/s, and the valley value increases from 0.49 kg/s to 0.83 kg/s. Figure 20 shows the average oil discharge flow rate carve and flow pulsation curve with different plunger

chamber radii and rotation speeds. By increasing the plunger chamber radius and correspondingly reducing the rotation speed, the filling rate of the plunger chamber is increased and the backflow is reduced because the cavitation in the plunger chamber is suppressed, thereby increasing the actual flow rate and reducing the flow pulsation rate. When the plunger chamber radius increases from 0.00925 m to 0.0105 m, the actual flow rate increases from 1.157 kg/s to 1.194 kg/s, and the flow pulsation rate decreases from 4.7% to 1.7%. To sum up, under the condition of a constant theoretical flow rate, by increasing the plunger chamber radius and correspondingly reducing the rotation speed, the cavitation in the plunger chamber can be effectively suppressed, the oil discharge flow rate is increased, and the flow pulsation rate is reduced, which can improve the stability and prolong the life of pumps.

4. Conclusions

In this paper, the axial piston pump is taken as the research object, and the research on suppressing cavitation, reducing flow pulsation, and increasing the actual flow rate is carried out by theoretical analysis, numerical calculation, and experimental test. By deriving the pressure drop equation of the plunger chamber considering the window pressure loss, it is found that the cavitation of the plunger chamber can be suppressed by reducing the swash plate inclination angle, reducing the cylinder rotation speed, reducing the distribution circle radius, and reducing the plunger chamber radius. However, the theoretical flow rate will be reduced when these methods are used to suppress cavitation in the plunger chamber, which has no practical engineering significance. In order to suppress the gaseous cavitation and vaporous cavitation in the plunger chamber under the condition of a constant theoretical flow rate, a model for suppressing cavitation in the plunger chamber with a constant theoretical flow rate is innovatively established by combining the flow equation of the plunger pump and the pressure drop equation of the plunger chamber. Based on this model, two methods for suppressing cavitation in the plunger chamber with an invariable theoretical flow rate are proposed. The first method is to increase the distribution circle radius and correspondingly reduce the rotation speed. The second method is to increase the plunger chamber radius and correspondingly reduce the rotation speed. Through the numerical calculation of the CFD model of the plunger pump and the flow rate test of the plunger pump at different pressures and speeds, the effectiveness of the two methods in suppressing cavitation of the plunger chamber, increasing the actual flow rate, and reducing the flow pulsation is further verified. The two methods of suppressing cavitation in the plunger chamber have important reference significance for the design and manufacture of axial plunger pumps.

Data Availability

The test data used to support the findings of this study are included within the article.

Conflicts of Interest

The authors declared no potential conflicts of interest with respect to the research, authorship, and/or publication of this article.

References

[1] Q. Chao, J. Zhang, B. Xu, H. Huang, and J. Zhai, "Centrifugal effects on cavitation in the cylinder chambers for high-speed axial piston pumps," *Meccanica*, vol. 54, no. 6, pp. 815–829, 2019.

[2] J. Ivantysyn and M. Ivantysynova, *Hydrostatic pumps and motors: principles, designs, performance, modeling, analysis, control and testing*, Tech Books Internationa, 2003.

[3] H. Ding, F. C. Visser, Y. Jiang, and M. Furmanczyk, "Demonstration and validation of a 3D CFD simulation tool predicting pump performance and cavitation for industrial applications," *Journal of Fluids Engineering*, vol. 133, no. 1, article 011101, 2011.

[4] G. E. Totten, Y. H. Sun, R. J. Bishop, and X. Lin, "Hydraulic system cavitation: a review," *SAE Transaction*, vol. 107, pp. 368–380, 1998.

[5] A. Yamaguchi and T. Takabe, "Cavitation in an axial piston pump," *Bulletin of JSME*, vol. 26, no. 211, pp. 72–78, 1983.

[6] T. Tsukiji, K. Nakayama, and K. Saito, "Study on the cavitating flow in an oil hydraulic pump," in *2011 International Conference on Fluid Power and Mechatronics*, pp. 253–258, Beijing, China, 2011.

[7] T. Tsukiji, Z. Chen, and J. J. Chen, "Visualized analysis of cavitation inside axial piston pump," *Chinese Hydraulics & Pneumatics*, vol. 2, pp. 1–7, 2015.

[8] O. Meincke and R. Rahmfeld, "Measurements, analysis and simulation of cavitation in an axial piston pump," in *6th International Fluid Power Conference*, pp. 485–499, TU Dresden, 2008.

[9] K. A. Edge and J. Darling, "Cylinder pressure transients in oil hydraulic pumps with sliding plate valves," *Proceedings of the Institution of Mechanical Engineers, Part B: Journal of Engineering Manufacture*, vol. 200, no. 1, pp. 45–54, 1986.

[10] R. M. Harris, K. A. Edge, and D. G. Tilley, "The suction dynamics of positive displacement axial piston pumps," *Journal of Dynamic Systems, Measurement, and Control*, vol. 116, no. 2, pp. 281–287, 1994.

[11] M. Liu, L. Tan, and S. L. Cao, "Cavitation–vortex–turbulence interaction and one-dimensional model prediction of pressure for hydrofoil ALE15 by large Eddy simulation," *Journal of Fluids Engineering*, vol. 141, no. 2, article 021103, 2018.

[12] Q. Chao, *Research on some Key Technologies of High Speed Rotation for Axial Piston Pump Used in EHAs*, ZheJiang University, 2019.

[13] C. G. Fey, G. E. Totten, R. J. Bishop, and A. Ashraf, "Analysis of common failure modes of axial piston pumps," SAE Technical Paper 2000; 2000-01-2581.

[14] M. Liu, L. Tan, and S. L. Cao, "Dynamic mode decomposition of cavitating flow around ALE 15 hydrofoil," *Renewable Energy*, vol. 139, pp. 214–227, 2019.

[15] W. Sun and L. Tan, "Cavitation-vortex-pressure fluctuation interaction in a centrifugal pump using bubble rotation modified cavitation model under partial load," *Journal of Fluids Engineering*, vol. 142, no. 5, article 051206, 2020.

[16] F. L. Yin, S. L. Nie, S. H. Xiao, and W. Hou, "Numerical and experimental study of cavitation performance in sea water hydraulic axial piston pump," *Proceedings of the Institution of Mechanical Engineers*, vol. 230, no. 8, pp. 716–735, 2016.

[17] J. H. Zhang, S. Q. Xia, S. G. Ye et al., "Experimental investigation on the noise reduction of an axial piston pump using free-layer damping material treatment," *Applied Acoustics*, vol. 139, pp. 1–7, 2018.

[18] K. Ito, K. Inoue, and K. Saito, "Visualization and detection of cavitation in V-shaped groove type valve plate of an axial piston pump," *Proceedings of the JFPS International Symposium on Fluid Power*, vol. 1996, no. 3, pp. 67–72, 1996.

[19] H. Ding, F. C. Visser, Y. Jiang, and M. Furmanczyk, "Demonstration and validation of a 3-D CFD simulation tool predicting pump performance and cavitation for industrial applications," *Journal of Fluids Engineering*, vol. 133, no. 1, article 011101, 2011.

[20] C. Schleihs, E. Viennet, M. Deeken et al., "3D-CFD simulation of an axial piston displacement unit," in *9th International Fluid Power Conference*, pp. 332–343, Aachen, Germany, 2014.

[21] P. Casioli, R. Vacca, and G. Franzoni, "Modelling of fluid properties in hydraulic positive displacement machines," *Simulation Modelling Practice and Theory*, vol. 14, no. 8, pp. 1059–1072, 2006.

[22] A. Vacca, R. Klop, and M. Ivantysynova, "A numerical approach for the evaluation of the effects of air release and vapour cavitation on effective flow rate of axial piston machines," *International Journal of Fluid Power*, vol. 11, no. 1, pp. 33–45, 2010.

[23] S. Gullapalli, P. Michael, J. Kensler, M. Cheekolu, R. I. Taylor, and E. Lizarraga-Garcia, "An investigation of hydraulic fluid composition and aeration in axial piston pump," in *Fluid Power Systems Technology*, vol. 58332, American Society of Mechanical Engineers, 2017.

[24] X. Y. Suo, Y. Jiang, and W. J. Wang, "Hydraulic axial plunger pump: gaseous and vaporous cavitation characteristics and optimization method," *Engineering Applications of Computational Fluid Mechanics*, vol. 15, no. 1, pp. 712–726, 2021.

[25] W. Kollek, Z. Kudźma, M. Stosiak, and J. Mackiewicz, "Possibilities of diagnosing cavitation in hydraulic systems," *Archives of Civil and Mechanical Engineering*, vol. 7, no. 1, pp. 61–73, 2007.

[26] G. E. Totten and R. J. Bishop, "The hydraulic pump inlet condition: impact on hydraulic pump cavitation potential," No. 1999-01-1877. SAE Technical Paper, 1999.

[27] N. D. Manring, V. S. Mehta, B. E. Nelson, K. J. Graf, and J. L. Kuehn, "Scaling the speed limitations for axial-piston swash-plate type hydrostatic machines," *Journal of Dynamic Systems Measurement & Control*, vol. 136, no. 3, article 031004, 2014.

[28] M. Kunkis and J. Weber, "Experimental and numerical assessment of an axial piston pump's speed limit," in *Fluid Power Systems Technology*, vol. 50060, American Society of Mechanical Engineers, 2016.

[29] R. J. Bishop and G. E. Totten, "Effect of pump inlet conditions on hydraulic pump cavitation: a review," *ASTM Special Technical Publication*, vol. 1339, pp. 318–332, 2001.

[30] C. J. Liu, X. F. Wu, and W. M. Gan, "Numerical simulation of cavitation flow in piston pump based on full cavitation model," *China Mechanical Engineering*, vol. 26, no. 24, pp. 3341–3347, 2015.

[31] N. Bügener, J. Klecker, and J. Weber, "Analysis and improvement of the suction performance of axial piston pumps in swash plate design," *International Journal of Fluid Power*, vol. 15, no. 3, pp. 1–15, 2014.

[32] G. Mohn and T. Nafz, "Swash plate pumps - the key to the future," in *10th International Fluid Power Conference*, pp. 139–150, Dresden, 2016.

[33] N. Bügener and J. Klecker, "Analysis of the suction performance of axial piston pumps by means of computational fluid dynamics (CFD)," in *The 7th International Fluid Power Conference*, pp. 641–654, Aachen, Germany, 2010.

[34] Q. Chao, J. Zhang, B. Xu, H. Huang, and J. Zhai, "Effects of inclined cylinder ports on gaseous cavitation of high-speed electro-hydrostatic actuator pumps: a numerical study," *Engineering Applications of Computational Fluid Mechanics*, vol. 13, no. 1, pp. 245–253, 2019.

[35] D. Gao, X. Suo, Q. Cai, S. Wu, and Y. Liang, "Influence of key structural parameters of hydraulic piston pump on cavitation in pump," *China Mechanical Engineering*, vol. 29, no. 4, pp. 434–440, 2018.